Journal Pre-proof

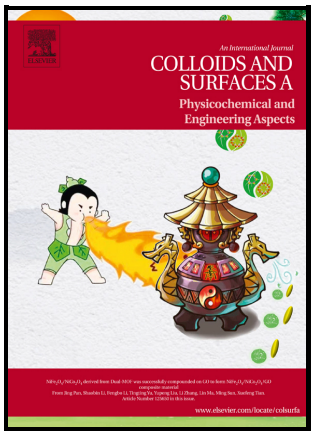

Experimental and theoretical studies of the interaction of ketoprofen in halloysite nanotubes

Dounia Sid, Milad Baitiche, Riadh Bourzami, Roufaida Merir, Ferhat Djerboua, Antonio Gil, Mokhtar Boutahala

PII: S0927-7757(21)01005-0

DOI: https://doi.org/10.1016/j.colsurfa.2021.127136

Reference: COLSUA127136

To appear in: *Colloids and Surfaces A: Physicochemical and Engineering Aspects*

Received date: 12 May 2021
Revised date: 28 June 2021
Accepted date: 4 July 2021

Please cite this article as: Dounia Sid, Milad Baitiche, Riadh Bourzami, Roufaida Merir, Ferhat Djerboua, Antonio Gil and Mokhtar Boutahala, Experimental and theoretical studies of the interaction of ketoprofen in halloysite nanotubes, *Colloids and Surfaces A: Physicochemical and Engineering Aspects,* (2021) doi:https://doi.org/10.1016/j.colsurfa.2021.127136

Experimental and theoretical studies of the interaction of ketoprofen in halloysite nanotubes

Dounia Sid[1, 2], Milad Baitiche[1], Riadh Bourzami[3], Roufaida Merir[1], Ferhat Djerboua[1], Antonio Gil[4] and Mokhtar Boutahala[2,*]

[1]*Laboratory of Multiphasic and Polymeric Materials, Department of Process Engineering, Faculty of Technology, University of Ferhat Abbas Setif-1, 19000 Setif, Algeria*

[2]*Laboratory of Chemical Process Engineering, Department of Process Engineering, Faculty of Technology, University of Ferhat Abbas Setif-1, 19000 Setif, Algeria*

[3]*Research Unit on Emergent Materials, University of Ferhat Abbas Setif-1, 19000 Setif, Algeria*

[4] *INAMAT^2, Science Department, Los Acebos Building, Public University of Navarra, Campus of Arrosadía, 31006, Pamplona, Spain*

E-mail: siddounia@univ-setif.dz(D. SID).

E-mail:baitiche_milad@yahoo.fr (M. BAITICHE).

E-mail: riadh_bourzami@hotmail.com (R. BOURZAMI).

E-mail : meroufaida@gmail.com (R. MERIR)

E-mail: ferhatdjerbouaf@gmail.com(F. DJERBOUA).

E-mail: andoni@unavarra.es (A. Gil)

[*]Corresponding author: E-mail: mboutahala@yahoo.fr (MBOUTAHALA).

Abstract

In recent years, the application of halloysite (HAL) in the conception of drug systems has become important due to its excellent physicochemical properties. Ketoprofen (KET) is widely used around the world as an anti-inflammatory drug. A formulation of HAL-KET was prepared. The interaction between the KET molecules and HAL has been investigated experimentally by Zeta potential, TEM, XRD, FTIR spectroscopy and TGA/DSC. In addition, this interaction was studied theoretically by using Monte-Carlo calculation method (MC). The results have shown that the interaction of KET is stabilized not only by electrostatic interactions and hydrogen bonds with HAL but also via the delocalized π electrons density of phenyl groups of KET and the hydrogen atoms of HAL.

Keywords**:** Halloysite; Ketoprofen; interaction; Characterization; Molecular modeling; Pharmaceutical carrier

1. Introduction

Ketoprofen (KET) is well known by its analgesic, anti-inflammatory and antipyretic properties. It is indicated mainly for the symptomatic treatment of pain and inflammation of osteoarthritis and rheumatoid arthritis **[1]**. The main drawbacks for the KET are low bioavailability, large number of gastro intestinal side effects, short biological half-life and poor-water solubility **[2]**. Many researchers made attempts to solve these problems by designing new carriers to achieve controlled and prolonged release property **[3–6]**.

Halloysite (HAL) is a clay mineral, physically and chemically analogous to kaolinite. HAL is characterized by a hollow nanotubular structure and composed by rolled kaolinite sheets **[7]**. The external diameter of the HAL tubes is from 50 to 200 nm with an internal diameter of 5 to 30 nm and a length of 0.5 to 25 μm. HAL nanotubes contain multiple rolled aluminosilicate layers **[8]**. HAL mainly occurs in two different form, the hydrated form (basal distance around 1.0 nm) with the formula $Al_2Si_2O_5$ $(OH)_4.nH_2O$ and the dehydrated form (basal distance about 0.7 nm) with the formula $Al_2Si_2O_5(OH)_4$, identical to kaolinite. The outer surface of HAL nanotubes is composed mainly of negatively charged SiO_2 and an inner surface composed of positively charged Al_2O_3. In addition, HAL nanotubes have a high specific surface area, good thermal stability, low cost and ability of loading drugs **[9–12]**. From these characteristics, HAL nanotubes have been widely used as supports for the loading and release of pharmaceutical agents as: 5-aminosalicylic acid **[13]**, ibuprofen **[14]**, diclofenac [**15]**, dexamethasone**[16]**, nifedipine **[17]**, furosemide **[18]**, resveratrol **[19]**, diphenhydramine **[20]**, 5-fluorouracil **[21],** paclitaxel **[22]**, isoniazide **[23],** irinotecan **[24]**, Pyrazole [3,4-*d*] pyrimidine derivatives **[25],** but not much molecular modelling work has been done on the mechanism of interaction of these pharmaceutical agents and HAL nanotubes.

Molecular modeling is a method that has been used to predict the mechanism of interaction between molecules with solid surfaces **[26]**, such as the mechanisms of adsorption of metals, organic compounds or biomolecules on mineral surfaces. In the pharmaceutical field, molecular simulations have been used to study the mechanisms and interactions between therapeutically active species and biologically inactive materials that can be used as carriers in drug delivery systems **[27]**.

This work will focus on the physico-chemical characterization of KET, HAL and KET loaded HAL (HAL-KET) by TEM, XRD, FTIR and TGA/DSC techniques and will specify the interaction energies of KET on HAL adsorption sites in the presence and absence of water by applying the Monte-Carlo calculation method (MC) and we will correlate between the

experimental results and those obtained by MC method. To our best knowledge, the study of the interaction between KET and HAL has not been previously reported.

2. Materials and Methods

2.1. Materials

The raw halloysite sample was directly collected from a mine of Djebbel Debbagh (Guelma, Algeria), ground, sieved and dried at 100°C for 24 h. The product was labeled as HAL-R. The drug ketoprofen (abbreviated as KET) (Formula: $C_{16}H_{14}O_3$, CAS number 22071-45-4, M_W: 254.3 g/mol, pKa=4.4, log K_{OW}=3.00, solubility in water at 25°C (S_W=21mg/L)) was supplied from SALEM Laboratories El-Eulma, Algeria. All reagents are used as received.

2.2. Halloysite Purification

In order to purify the HAL-R [**28]**, 20 g of this sample is dispersed in 1L of distilled water and stirred for 24 h and then centrifuged at 5000 rpm for 5 min. The obtained precipitate was washed with 2 L of 0.1 M HCl under strong agitation and at room temperature for 4 h in order to remove the carbonates. Afterward, the obtained precipitate was repeatedly washed with distilled water and centrifuged successively for at least five centrifugations until the supernatant became neutral. For removing the organic matter, the solid residue is added to a solution of oxygenated water (10% v/v) and stirred overnight at room temperature. Then, the residual hydrogen peroxide is degraded by heating under the temperature of 70 °C for 30 min. The precipitate is washed with hot water and dried at 60°C for 24 h and stored in bottles. The resultant sample was denoted as HAL.

2.3. Ketoprofen loading

In order to obtain a saturated solution, 1g of KET was added in 250 mL of water. Then, 1 g of HAL was dispersed into this solution and mixed to obtain a homogeneous suspension. The suspension was placed in vacuum for 4 cycles, each for 30 min allowing air bubbles to be removed from HAL pores, which is generally indicated by a slight fizzing of the solution. Once the vacuum is broken, the solution enters the lumen to ensure maximum loading [**29]**. The sample was removed and washed triply with 200 ml of water to remove excess drug not adsorbed. The sample denoted HAL-KET was dried at 60°C overnight and powdered**.**

2.4. Characterization techniques

The chemical composition of halloysite before and after purification was determined by X-ray fluorescence (XRF) using (Rigaku primus IV apparatus, Japan).

The zeta potential of the halloysite dispersion, versus pH, was measured using nano particle analyzer sz-100 (Horiba Scientific, Japan). In addition, the pH_{PZC} of halloysite was measured using the pH drift method **[30] (Fig. not shown).**

Nitrogen gas adsorption–desorption isotherms were measured using a Micromeritics Tristar 3000 instrument at 77 K. The measurements were made after degassing the samples under vacuum at 200°C for 3 h. The specific surface areas are determined according to the BET method at the relative pressure in the range of 0.05–0.35 **[31].** The total pore volume, V_{pore}, was directly determined from the Nitrogen adsorption at $P/P_o = 0.98$.

The analysis of the microstructures of HAL and HAL-KET were performed with Transmission Electronic Microscopy (TEM) using JEOL 1400 Flash apparatus, operating with an accelerating voltage of 120 kV. A droplet of 5µl of HAL nanoparticles dispersed in distilled water was deposited onto a carbon coated copper grid (CF200-CU UL EMS). Excess solution was carefully blotted off using filter paper and air-dried at room temperature during one night for imaging. To obtain right distributions, more than 100 halloysite crystals dimensions were considered.

The structure of HAL-R, HAL, KET and HAL-KET samples was determined by XRD measurement (Bruker D8 advance diffractometer operating at 40 kV as acceleration tension and 30 mA as courant with Cu Kα1 radiation (λ=0.1542 nm)). Radial scans were recorded in the reflection scanning mode from 5 to 80° (2θ) with a scanning rate of 10 ° ·min^{-1}. Bragg's law, defined as $n\lambda = 2d \sin\theta$, was used to compute the interreticular distances (d) for the examined clay samples.

The infrared spectra of HAL, KET and HAL-KET were obtained using Fourier transformed infrared spectroscopy (FTIR-8400S Shimadzu (Japan) spectrophotometer from 400 to 4000 cm^{-1}, using KBr pellets technique.

Loading efficiency was determined using thermogravimetric analysis (TGA/DSC) on an EXTAR 6000 thermal analyzer (Seiko, Mahwa, NJ, USA) under nitrogen atmosphere at heating rate of 10 °C min^{-1}, from 30 to 900 °C.

2.5. Calculation methods

The chemical calculations were performed employing three softwares, Gaussian 9.5 W, the Forcite modulus and the Adsorption locator modulus included in Materials Studio software packages.

The geometrical optimizations of the KET and the water molecules were carried out with Gaussian 9.5W based on the Density Functional theory (DFT) with Beck's three

parameter hybrid exchange Lee–Yang–Parr correlation (B3LYP) in conjunction with 6-31G (d, p) basis set **[32,33]**. Those parameters are well adapted for the small molecular structures **[34–36]**. To get more reliable data, the effect of the solvent was considered, which was defining as the water molecules.

The HAL has the same crystalline structure as kaolinite and morphologically, the planar form of HAL is comparable to that of kaolinite **[7]**. The lamellar kaolinite structure was developed using the crystallographic parameters defined in the AMCSD file 0012232. In order to develop the modeling of the adsorption, supercells of kaolinite (001) and (00-1) with the dimensions (1.5466 x 2.6834 x 1.1513 nm corresponding to 3 x 3 x 2 unit cells, these dimensions correspond to the ratio: 1 molecule of KET to 9 surface unit cell of kaolinite) **(Figure.1)** and 12 nm as vacuum slab are chosen which respecting the periodic boundary conditions at the interfaces. Those dimensions are largely sufficient to host the KET and the waters molecules. The geometrical optimization of the supercells was performed using Forcite modulus, based on classical theory; Universal Forcefield type and the ultrafine convergence criteria were used on basis set definitions.

Finally, the adsorption was modeled by the means of the canonical Molecular Dynamic Simulation (MDS), using adsorption locator modulus based on Monte Carlo (MC) theory, starting from the geometrical optimization of the pristine materials (KET and HAL substrate). A normal thermodynamic ensemble and a temperature of 25 ºC (this temperature is close to experimental one) were fixed. The equilibrium configurations were performed using the neutral charge of the both adsorbent and adsorbate, which considering the zero charge point of the system. The time step was 0.1 fs and the simulation time was 1 ns, moreover, the geometrical optimization of the adsorbed molecule was considered after 10 cycles and 100000 steps by cycle which taken at every step, $2*10^{-5}$Kcal·mol^{-1} as cut off energy, 10^{-3} Kcal·mol^{-1}.Å^{-1} as max. force and 10^{-6} nm as max. displacement. The adsorption was simulated in the vacuum slab under 1.2 nm distance from the substrate.

3. Results and discussion

3.1. Experimental investigation

Chemical analyses of halloysite before (HAL-R) and after purification (HAL) are listed in **Table 1.** Purification shows an increase in the content of SiO_2 and decrease in the content of Al_2O_3. The ratio of SiO_2/Al_2O_3 increased slightly from 1.20 to 1.29. The decrease in the alumina content in the HAL can be ascribed to the leaching of Al ions from the octahedral

layer due to hydrolysis under purification by acid. This dealumination is accompanied by the reduction of impurities CaO, Fe_2O_3, K_2O and MnO_2.

Zeta potential measurements of HAL (1g/L) are performed within the pH ranging from 2 to 11 **(Figure 2)**. This figure shows that the surface of the HAL was positively charged at very low pH and an increasingly negative value at the pH rises. The isoelectric point of HAL is around 3.6.

The adsorption- desorption isotherms of HAL-R and HAL are presented in **Figure 3**. The isotherms of these samples are classified as type IV isotherms with H3 hysteresis loops **[37].** This type of isotherm is a typical characteristic of mesopores structures. The S_{BET} and V_{pore} values of HAL-R and HAL are (150.3 m^2/g, 0.212 cm^3/g) and (191.2 m^2/g, 0.208 cm^3/g), respectively.

The TEM images of HAL and HAL-KET are shown in **Figure 4**. The TEM images of HAL **(Figures 4a-c)** consist of various sizes of nanotubular shapes, the length of the HAL is comprise from 40 to 1300 nm, this result conforms to the conventional values of these clay minerals that are comprised between 20 and 2000 nm **[7]**. After addition of KET, the central part of the HAL lumen and outer surface of the nanotubes became darker which proves that the KET molecules were adsorbed on the internal and external surfaces, respectively **(Figures 4d-f)**. **The Figures 5a-b** presents the distribution of the external diameters of HAL-KET and HAL. They show that deposit is almost homogeneous and the average external diameter estimated by the fit by Gaussian function is 35 ± 13 nm and 43 ± 13 nm with a width at mid-height of 25 and 25 nm respectively for HAL and HAL-KET. The estimated thickness of KET deposited on the outer surface in a homogeneous manner is about (43 - 35)/2= 4 nm. In addition, the **Figures 4d-f** shows that the lumen volume of HAL is filled by the KET molecules. In order to modulate the adsorption of KET into HAL, the average internal diameter of the empty volume of the nanotubes of HAL-KET and HAL (considering the deposit homogenous) is estimated **(Figs.6c-d)**.The found values respectively are 16± 3 nm and 8 ± 3 nm which were obtained from the fit by Gaussian function of the diameter distribution, so the estimation of the average deposited homogeneous thickness is about (16 - 8)/2 = 4 nm.

The XRD patterns of HAL-R, HAL, KET and HAL-KET are shown in **Fig.7**. According to the XRD patterns, the pattern of HAL shows the characteristic diffraction peaks at the angular positions 2θ=12.25, 20.24, 24.97, 35.27, 36.19, 55.31 and 62.59 °, corresponding respectively to the Miller indices of the reticular planes: (001), (020), (002), (003), (200), (211) and (-3-31**) [38]**. The crystalline phases of quartz, carbonate, alumina and

cristobalite are also observed in the HAL-R and HAL samples but in small quantities in a trace **[39,40]**.The interreticular distances $d_{(001)}$=0.723 and $d_{(020)}$= 0.440 nm are characteristic of the dehydrated phase of HAL ($Al_2Si_2O_5$) that has a tubular morphology **[7]**. Otherwise, the KET exhibits diffraction peaks at the angular positions 13.48, 14.78, 17.68, 23.25, 28.13 and 32.94 ° because its crystallinity However, these characteristic peaks disappeared in KET loaded HAL (HAL-KET) which indicates that the KET changes its state from crystalline to amorphous nature. These results show as well that KET molecules were diluted in the HAL structure. This conclusion is consistent with the previous studied on drug-loaded HAL [**14,41,42**]. In addition the KET is not intercalated between layers because the basal spacing of halloysite with KET anions is the same like in HAL sample, see **Fig.7.**

The interaction between KET and HAL was studied by FTIR spectroscopy, as shown in the **Fig.8**. The spectrum of the HAL shows two bands centered at 3692 and 3626 cm^{-1}, belonging to the hydroxyl region (3000–4000 cm^{-1}), they were attributed to the stretching vibrations of inner-surface of Al_2-OH groups and the deformation vibration of interlayer water, respectively. In addition, the wide bands centered at 3464 cm^{-1} and weak at 1639 cm^{-1} were attributed to the stretching and OH deformation vibration modes of the physically adsorbed water, respectively. The groups at 1090 and 1029 cm^{-1} correspond to the stretching vibrations of Si-O in the plane and Si-O-Si, respectively. The band at 916 cm^{-1} was attributed to the O-H deformation of the internal hydroxyl groups and that at 793 cm^{-1} was caused by a symmetrical stretching vibration of Si-O. The bands at 752 and 687 cm^{-1} were attributed to the perpendicular Si-O stretching vibrations. The three remaining bands at 540, 470 and 437 cm^{-1} can be attributed to the deformation vibrations of the groups Al-O-Si, Si-O-Si, and Si-O, respectively **[43]**. The FTIR spectrum of KET shows characteristic adsorption peaks at 3500 cm^{-1} due to O–H stretching and the bands at 2970 and 2930 cm^{-1} are due to C–H stretching asymmetric and symmetric of the methyl group respectively. Moreover, there was a stretching band at1698 cm^{-1} (for C=C stretching of carboxylic acid), 1654 cm^{-1} (for ketone group attached to two aromatic rings), 1598 cm^{-1} and 1440 cm^{-1} (for C=C stretching from the aromatic ring), 1321 cm^{-1} (for CH deformation of CH_3 symmetrical), 1281 cm^{-1} (for C=C deformation of aromatic rings) **[44]**. Regarding the FTIR spectrum of HAL-KET sample, it was clear that the characteristic peaks of HAL were maintained, the presence of new peaks at the frequencies 1691 cm^{-1} (C=C stretching of carboxylic acid), 1660 cm^{-1} (C=O group), 1450 cm^{-1} (C=C stretching from the aromatic ring) and 1290 cm^{-1}(C=C deformation of aromatic rings), belonging to KET, prove the interaction of KET with HAL. Comparative results were found during the intercalation of KET on mesoporous silica nanoparticles **[45]**.

The thermal gravimetric analysis curves (TGA) of the HAL, KET and HAL-KET samples obtained under nitrogen atmosphere are shown in **Fig.9**. The TGA analysis for the HAL shows two significant mass losses clearly observed. The first mass loss takes place from 25 to 400 °C attributed to the dehydration of physically adsorbed water and interlamelar residual water. The second loss of mass between 400 and 600 °C can be attributed to the dehydratation of hydroxyl groups (Al-OH and Si-OH groups on HAL) **[46]**. This result is comparable to that observed in the literature concerning the dehydroxylation of HAL between 400 and 600 °C **[47]**.The TGA curve of KET shows thermal decompositions between 217-394 °C with a single mass loss, centered at 319°C. The TGA profiles indicate that KET are stable up to 167 and that there are no mass losses for KET before this temperature. The thermogram of HAL-KET can be seen as a superposition of thermograms of the pristine materials. The mass losses of HAL in HAL-KET show the same profiles as that of pure HAL, however the degradation profiles of KET change. Loading efficiency of KET (wt %) was calculated by the difference between the total weight loss of KET loaded HAL and unloaded HAL samples. According to following formula: loading efficiency (%)= W_1-W_0 (where W_1 and W_0 represent the % weight loss of KET loaded into HAL and the weight loss of unloaded HAL at 450 °C, respectively. The total mass losses obtained at T=450 °C for HAL and HAL-KET are 7.04 % and 24.96 %, respectively. The loading efficiency of KET in HAL is estimated to be 17.92%. This amount adsorbed on internal and external surfaces of HAL is close to the HAL loaded by drugs mentioned in the literature **[29]**. It should be noted that the degradation temperature of KET in the HAL-KET determined by DSC is different than that of pure KET **(Fig.9 inset)**.The endothermic peak attributed to the KET melting in the HAL-KET sample shifts to lower values centered at 123 °C. The diminution of the value of the melting point may be attributed to the interaction of KET with HAL and the formation of amorphous phase of KET **[24,42]**, the low intensity of the signal is due probably to a dilution phenomenon. The XRD pattern of HAL-KET also confirms this claim where no peaks associated to KET were observed **(Fig.7)**.

3.2. Theoretical investigation

3.2.1. Equilibrium configurations

The MDS helps to find the most stable adsorption sites on external and internal kaolinite surfaces through minimization of the energy for each adsorption sites. The **Figure 10 shows** the equilibrium configurations of the ketoprofen and water molecules on kaolinite (001) and (00-1) surfaces, the external atomic layer illustrated by yellow color, is selected for

the adsorption, and the **Table 2** summarizes their related output adsorption energies in kJ/mol, including, the total energy, the rigid adsorption energy, the deformation energy and dE_{ads}/dNi, the values of the energy were calculated taken the substrate energy as null.

The total energy is defined as the sum of the energies of the adsorbate molecules, it reports the energy released (or required) when the relaxed adsorbate molecules are adsorbed, it is defined as the sum of the rigid adsorption energy and the deformation energy. The rigid adsorption energy reports the energy released (or required) when the unrelaxed adsorbate molecules are adsorbed on the substrate. The deformation energy reports the energy released when the adsorbed adsorbate components are relaxed on the substrate surface. Finally, dE_{ads}/dNi is the energy of adsorbate-adsorbent configurations when one of the adsorbate molecules has been removed; the negative energy values indicate the spontaneity of the adsorption process.

The **Figure 10a** shows the most likely adsorption area of the water molecules projected on side and top views for the both surfaces, on the surface (001) the water molecule prefers the top sites of the oxygen atoms, while, the hollows are the most likely adsorption sites for water molecules on the surface (00-1). According to the equilibrium configurations presented in the **Figure 10b**, it can be seen that of the ketoprofen molecule is adsorbed in longitudinal configuration, such that at least one aromatic ring finds a quasi-planar configuration with respect to the surface of the substrate for both orientations (001) and (00-1). At the last, the **Figure 10c** exhibits the closest configuration from the experiments, taken in account the adsorption if the KET with 30 water molecules. **Figure 10c** illustrates that the longitudinal configuration is almost conserved, in another words, the water molecules don't influence the affinity of the adsorption of the ketoprofen.

3.2.2. Hydrogen bonding system

The equilibrium configurations illustrate a good affinity of the adsorption of the ketoprofen and water molecules on kaolinite (001) and (00-1) surfaces, the large distance between the adsorbate molecules and adsorbents surfaces substantiates the absence of covalent bonds, although weak bonds can be involved, where hydrogen bonds and van-der Waals-type dipolar electrostatic forces and π electrons interactions are mainly predominant.

The **Figure 11** shows the magnification of the adsorption contact provided by: the predicted extramolecular hydrogen bonding system, and by the distance between aromatic cycles of ketoprofen and the adsorbent surfaces.

For the surface (001), any hydrogen bonds below 3 Å of the distance H···Acceptor was predicted between the ketoprofen and this surface **(Fig.11d)**, and the distance between the longitudinal aromatic cycle and the surface is about 3.83 Å, at this distance, the short contact and the conjugated π electrons can be weakly involved in the adsorption mechanism, this result can be seen on the low the total adsorption energy of 3.286 kJ/ mol, otherwise, on this surface, the water molecules at the hollow sites can generate three hydrogen bonds between the oxygen of the water as donor and the oxygen of the adsorbent surface as acceptor **(Fig.11c)**, these three hydrogen bonds increase the total adsorption energy to the value -4.042 kJ/ mol.

For the adsorption on the surface (00-1), divers hydrogen bonds were predicted, this diversity may be related to the richness of this surface by the hydrogen. Two hydrogen bonds accurate between the oxygen of the surface as donor and the oxygen of the ketoprofen as acceptor, and another one between the oxygen of the hydroxyl group of the ketoprofen as donor and the oxygen of the surface as acceptor **(Fig.11b)**. In addition, the minimum distance between the longitudinal cycle and surface is about 3.17 Å, at this distance, the short contact and the π-electrons are involved in the adsorption mechanism, the total adsorption energy in this situation is 3.741 kJ/ mol. Finally, the adsorption of water molecule on this adsorbent surface occurs through one weak hydrogen bond between the oxygen of the surface as donor and the oxygen of water as acceptor **(Fig.11a)** with energy of -4,042 kJ/ mol. The **Table 3** summarizes the corresponding acceptor-donor bond lengths and angles measurements characteristic of the predicted hydrogen bonds.

3.3. Suggested adsorption mechanism

In this work, HAL was used as a drug carrier for the loading of KET by vacuum method. The use of vacuum to improve the loading efficacy into the halloysite nanotubes is well established experimentally but its interpretation has been reported recently. Of course, due to capillarity the nanotubes are quickly filled and there is no need for vacuum to remove air from inside **[48].** The mechanism of interaction of KET with HAL was evaluated by zeta potential, XRD, TEM, TGA / DSC and FTIR. After loading the HAL nanotubes with KET, the FTIR spectrum showed the appearance of new absorption peaks attributed to the KET molecules. According to TEM images, KET was mainly encapsulated in the lumen and loaded on the external surface of halloysite. The loading efficiency of KET introduced into HAL is 17.92%. But by DRX, no peaks relative to KET were observed, suggesting that the state of KET in HAL is in an amorphous state. As the zeta potential of HAL is between 3 and 4, this indicates that HAL is positive in the acidic medium and negative beyond pH greater than 3.6.

On the other hand, KET presents a negative charge at pH = 7.4 and a positive charge at pH = 4 **[49].** Knowing that the oxygen of the carbonyl function and that of the carboxylic acid one are more electronegative than the carbon atoms, this will lead to the development positive charges on the KET molecule**.** To this the effect of conjugation due to the aromatic rings can be added. This might increase the probability of creating positive charges on the drug particles **[49].** The mechanism of interaction of KET in HAL nanotubes is determined by the functional groups existing on the surface which are Si-OH (electronegative), Al-OH (electropositive), and some Al-OH and Si-OH groups are located on surface defects of halloysite. These hydroxyl groups allow halloysite to carry a pH-dependent surface charge **[50].** The adsorption mechanism between the KET molecule and the surface can be proposed as follows:

1/ Electrostatic interactions

- Between the positive groups of the KET and the deprotonated silanols ($Si\text{-}O^-$) and ($Al\text{-}O^-$) located on surface defects of halloysite
- between the negative groups of the KET and the Al-OH of lumen surface
- Between the delocalized π electron density of benzene rings drug and the hydrogen atoms of the tetrahedral layer of Hal clay.

2/ Hydrogen bonds

- Between the hydrogen of the hydroxyl group of the KET and the oxygen atoms of the tetrahedral layer ($Si\text{-}O^-$) of HAL surface.
- Between the oxygen atoms of the KET and the hydrogen atoms of the surface.

4. Conclusion

The present work reports the use of Algerian halloysite as a carrier for the loading of KET molecules. Physicochemical characterizations show that the KET was mainly loaded in internal and external surfaces of halloysite, respectively, and that ketoprofen is present in amorphous phase in HAL-KET composite. The TGA profiles show that the loading efficiency of KET introduced into HAL is 17.92%. This amount of KET is distributed homogeneously on the outer surface and in a non-homogeneous manner on the inner surface of the nanotubes. The study by Monte-Carlo theory illustrates a good affinity for adsorption of KET on the inner and outer surfaces, and these affinities of adsorption are not significantly influenced by the presence of water molecules. The mechanism of interaction of KET with HAL is physical, where several hydrogen bonds and electrostatic interaction are predominant.

Acknowledgments

This work was generously supported by la direction générale de la recherche scientifique (Algeria) et le laboratoire de génie des procédés chimiques (LGPC) de l'université de Sétif 1. A.G also thanks Santander Bank (Navarra, Spain) for funding via the Research Intensification Program.

References

[1]T.G. Kantor, Ketoprofen: A Review of Its Pharmacologic and Clinical Properties, Pharmacotherapy: The Journal of Human Pharmacology and Drug Therapy. 6 (1986) 93–102. https://doi.org/10.1002/j.1875-9114.1986.tb03459.x.

[2]S. Rençber, S.Y. Karavana, M. Özyazici, Bioavailability file: ketoprofen, FABAD Journal of Pharmaceutical Sciences. 34 (2009) 203.

[3]M. Kaleemullah, K. Jiyauddin, E. Thiban, S. Rasha, S. Al-Dhalli, S. Budiasih, O.E. Gamal, A. Fadli, Y. Eddy, Development and evaluation of Ketoprofen sustained release matrix tablet using Hibiscus rosa-sinensis leaves mucilage, Saudi Pharmaceutical Journal. 25 (2017) 770–779. https://doi.org/10.1016/j.jsps.2016.10.006.

[4]E.D. de Freitas, P.C.P. Rosa, M.G.C. da Silva, M.G.A. Vieira, Development of sericin/alginate beads of ketoprofen using experimental design: Formulation and in vitro dissolution evaluation, Powder Technology. 335 (2018) 315–326. https://doi.org/10.1016/j.powtec.2018.05.016.

[5]M.V. Harsha, S.R. Baratam, A.K. Kishore, Development and Evaluation of Ketoprofen Sustained delivery system using NeemGum, Research Journal of Pharmacy and Technology. 14 (2021) 817–822. https://doi.org/10.5958/0974-360X.2021.00144.X.

[6]M. Kamada, F. Hirayama, K. Udo, H. Yano, H. Arima, K. Uekama, Cyclodextrin conjugate-based controlled release system: repeated- and prolonged-releases of ketoprofen after oral administration in rats, Journal of Controlled Release. 82 (2002) 407–416. https://doi.org/10.1016/S0168-3659(02)00171-2.

[7]E. Joussein, S. Petit, J. Churchman, B. Theng, D. Righi, B. Delvaux, Halloysite clay minerals - a review, Clay Minerals. 40 (2005) 383–426. https://doi.org/10.1180/0009855054040180

[8]R. Yendluri, Y. Lvov, M.M. de Villiers, V. Vinokurov, E. Naumenko, E. Tarasova, R. Fakhrullin, Paclitaxel Encapsulated in Halloysite Clay Nanotubes for Intestinal and Intracellular Delivery, Journal of Pharmaceutical Sciences. 106 (2017) 3131–3139. https://doi.org/10.1016/j.xphs.2017.05.034.

[9]M. Liu, Z. Jia, D. Jia, C. Zhou, Recent advance in research on halloysite nanotubes polymer nanocomposite, Progress in Polymer Science. 39 (2014) 1498–1525. https://doi.org/10.1016/j.progpolymsci.2014.04.004.

[10]B. Wu, M. Jiang, X. Liu, C. Huang, Z. Gu, Y. Cao, Evaluation of toxicity of halloysite nanotubes and multi-walled carbon nanotubes to endothelial cells in vitro and blood vessels in vivo,Nanotoxicology.14 (2020) 1017–1038. https://doi.org/10.1080/17435390.2020.1780642.

[11]N. Alipoormazandarani, S. Ghazi hoseini, A. Mohammadi Nafchi, Preparation and characterization of novel bionano composite based on soluble soybean polysaccharide and halloysite nanoclay, Carbohydrate Polymers. 134 (2015) 745–751. https://doi.org/10.1016/j.carbpol.2015.08.059.

[12]S. Leporatti, Halloysite clay nanotubes as nano-bazookas for drug delivery, Polymer International. 66 (2017) 1111–1118. https://doi.org/10.1002/pi.5347.

[13]C. Aguzzi, C. Viseras, P. Cerezo, I. Salcedo, R. Sánchez-Espejo, C. Valenzuela, Release kinetics of 5-aminosalicylic acid from halloysite, Colloids and Surfaces B: Biointerfaces. 105 (2013) 75–80. https://doi.org/10.1016/j.colsurfb.2012.12.041.

[14]D. Tan, P. Yuan, F. Annabi-Bergaya, H. Yu, D. Liu, H. Liu, H. He, Natural halloysite nanotubes as mesoporous carriers for the loading of ibuprofen, Microporous and Mesoporous Materials. 179 (2013) 89–98. https://doi.org/10.1016/j.micromeso.2013.05.007.

[15]L. Lisuzzo, G. Cavallaro, S. Milioto, G. Lazzara, Layered composite based on halloysite and natural polymers: a carrier for the pH controlled release of drugs, New J. Chem. 43 (2019) 10887–10893. https://doi.org/10.1039/C9NJ02565K.

[16]N. G. Veerabadran, R. R. Price, Y. M. Lvov, Clay nanotubes for encapsulation and sustained release of drugs, NANO. 02 (2007) 115–120. https://doi.org/10.1142/S1793292007000441.

[17]R. Yendluri, D.P. Otto, M.M. De Villiers, V. Vinokurov, Y.M. Lvov, Application of halloysite clay nanotubes as a pharmaceutical excipient, International Journal of Pharmaceutics. 521 (2017) 267–273. https://doi.org/10.1016/j.ijpharm.2017.02.055.

[18]M. Hanif, F. Jabbar, S. Sharif, G. Abbas, A. Farooq, M. Aziz, Halloysite nanotubes as a new drug-delivery system: a review, Clay Minerals. 51 (2016) 469–477 https://doi.org/10.1180/claymin.2016.051.3.03.

[19] V. Vergaro, Y.M. Lvov, S. Leporatti, Halloysite Clay Nanotubes for Resveratrol Delivery to Cancer Cells, Macro-molecular Bioscience. 12 (2012) 1265–1271. https://doi.org/10.1002/mabi.201200121.

[20] H. Hemmatpour, V. Haddadi-Asl, H. Roghani-Mamaqani, Synthesis of pH-sensitive poly (N,N-dimethyl amino ethyl methacrylate)-grafted halloysite nanotubes for adsorption and controlled release of DPH and DS drugs, Polymer. 65 (2015) 143–153. https://doi.org/10.1016/j.polymer.2015.03.067.

[21] S. Harikrishnan, R. Sedev, C.C. Beh, C. Priest, N.R. Foster, Loading of 5-fluorouracil onto Halloysite nanotubes for targeted drug delivery using a subcritical gas antisolvent process (GAS), The Journal of Supercritical Fluids. 159 (2020) 104756. https://doi.org/10.1016/j.supflu.2020.104756.

[22] A. Borrego-Sánchez, M.E. Awad, C.I. Sainz-Díaz, Molecular Modeling of Adsorption of 5-Aminosalicylic Acid in the Halloysite Nanotube, Minerals. 8 (2018) 61. https://doi.org/10.3390/min8020061.

[23]E. Carazo1, A. Borrego-Sánchez1,2, F. García-Villén1, R. Sánchez-Espejo1, C. Aguzzi1, C.Viseras1,2, C.I. Sainz-Díaz2, P. Cerezo1, Assessment of halloysite nanotubes as vehicles of isoniazid, Colloids and Surfaces B: Biointerfaces Volume 160, 2017, Pages 337-344. https://doi.org/10.1016/j.colsurfb.2017.09.036

[24] Eleni Giannia,c, Konstantinos Avgoustakisb, Milan Pšeničkac, Miroslav Pospíšilc, Dimitrios Papoulisa, Halloysite nanotubes as carriers for irinotecan: Synthesis and characterization by experimental and molecular simulation methods, Journal of Drug Delivery Science and Technology, Journal of Drug Delivery Science and Technology 52 (2019) 568–576. https://doi.org/10.1016/j.jddst.2019.05.001

[25]Marina Massaro, Giampaolo Barone, Viviana Barra, Patrizia Cancemi, Aldo Di Leonardo, Giancarlo Grossi, Fabrizio Lo Celso, Silvia Schenone, Cesar Viseras Iborra Serena Riela, Pyrazole[3,4-*d*] pyrimidine derivatives loaded into halloysite as potential CDK inhibitors, International Journal of Pharmaceutics 599 (2021) 120281. https://doi.org/10.1016/j.ijpharm.2021.120281

[26] D. Sid, M. Baitiche, Z. Elbahri, F. Djerboua, M. Boutahala, Z. Bouaziz, M.L. Borgne, Solubility enhancement of mefenamic acid by inclusion complex with β-cyclodextrin: in silico modelling, formulation, characterisation, and in vitro studies, Journal of Enzyme Inhibition and Medicinal Chemistry. 36 (2021) 605–617. https://doi.org/10.1080/14756366.2020.1869225.

[27] S. Karimzadeh, B. Safaei, T.-C. Jen, Theorical investigation of adsorption mechanism of doxorubicin anticancer drug on the pristine and functionalized single-walled carbon nanotube surface as a drug delivery vehicle: A DFT study, Journal of Molecular Liquids. 322 (2021) 114890. https://doi.org/10.1016/j.molliq.2020.114890.

[28] Handbook of Clay Science, second edition, part B: Techniques and Applications Edited by F. Bergaya and G. Lagaly,2013.

[29] E. Abdullayev, Y. Lvov, Chapter 22 - Halloysite for Controllable Loading and Release, in: P. Yuan, A. Thill, F. Bergaya (Eds.), Developments in Clay Science, Elsevier, 2016: pp. 554–605. https://doi.org/10.1016/B978-0-08-100293-3.00022-4.

[30] Sahnoun, S., Boutahala, M., Zaghouane-Boudiaf, H., Zerroual, L., Trichlorophenol removal from aqueous solutions by modified halloysite: kinetic and equilibrium studies. Desalination and Water Treatment 57 (2016)15941-15951. https://doi.org/10.1080/19443994.2015.1075159

[31]S. Brunauer, P. H. Emmett, E. Teller, J. Am. Chem. Soc. 60 (1938) 309

[32] C. Lee, W. Yang, R.G. Parr, Development of the Colle-Salvetti correlation-energy formula into a functional of the electron density, Phys. Rev. B. 37 (1988) 785–789. https://doi.org/10.1103/PhysRevB.37.785.

[33] B. Miehlich, A. Savin, H. Stoll, H. Preuss, Results obtained with the correlation energy density functionals of becke and Lee, Yang and Parr, Chemical Physics Letters. 157 (1989) 200–206. https://doi.org/10.1016/0009-2614(89)87234-3.

[34] Y. Nishiyama, P. Langan, H. Chanzy, Crystal Structure and Hydrogen-Bonding System in Cellulose Iβ from Synchrotron X-ray and Neutron Fiber Diffraction, J. Am. Chem. Soc. 124 (2002) 9074–9082. https://doi.org/10.1021/ja0257319.

[35] L. Ouksel, S. Chafaa, R. Bourzami, N. Hamdouni, M. Sebais, N. Chafai, Crystal structure, vibrational, spectral investigation, quantum chemical DFT calculations and thermal behavior of Diethyl [hydroxy (phenyl) methyl] phosphonate, Journal of Molecular Structure. 1144 (2017) 389–395.https://doi.org/10.1016/j.molstruc.2017.05.029.

[36] R. Bourzami, L. Ouksel, N. Chafai, Synthesis, spectral analysis, theoretical studies, molecular dynamic simulation and comparison of anticorrosive activity of an ester and an acid α-Hydroxyphosphonates, Journal of Molecular Structure. 1195 (2019) 839–849. https://doi.org/10.1016/j.molstruc.2019.06.012.

[37]S. J. Gregg, K. S. W. Sing, Adsorption, surfaces area and porosity. Academic Press. London, (1982)

[38] G. Brown, Crystal Structures of Clay Minerals and their X-Ray Identification, The Mineralogical Society of Great Britain and Ireland, 1982.

[39] A. Aras, The change of phase composition in kaolinite- and illite-rich clay-based ceramic bodies, Applied Clay Science. 24 (2004) 257–269. https://doi.org/10.1016/j.clay.2003.08.012.

[40] S.R. Levis, P.B. Deasy, Characterization of halloysite for use as a microtubular drug delivery system, International Journal of Pharmaceutics. 243 (2002) 125–134. https://doi.org/10.1016/S0378-5173(02)00274-0.

[41] O. Sreekanth Reddy , M.C.S. Subha , T. Jithendra , C. Madhavi , K. Chowdoji Rao, Curcumin encapsulated dual cross linked sodium alginate/montmorillonite polymeric composite beads for controlled drug delivery, Journal of Pharmaceutical Analysis 11 (2021) 191-199. https://doi.org/10.1016/j.jpha.2020.07.002

[42] D. Tan, P. Yuan, F. Annabi-Bergaya, D. Liu, L. Wang, H. Liu, H. He, Loading and in vitro release of ibuprofen in tubular halloysite, Applied Clay Science. 96 (2014) 50–55. https://doi.org/10.1016/j.clay.2014.01.018.

[43] H. Sabahi, M. Khorami, A.H. Rezayan, Y. Jafari, M.H. Karami, Surface functionalization of halloysite nanotubes via curcumin inclusion, Colloids and Surfaces A: Physicochemical and Engineering Aspects. 538 (2018) 834–840. https://doi.org/10.1016/j.colsurfa.2017.11.038.

[44] R. Soto, M. Svärd, V. Verma, L. Padrela, K. Ryan, Å.C. Rasmuson, Solubility and thermodynamic analysis of ketoprofen in organic solvents, International Journal of Pharmaceutics. 588 (2020) 119686. https://doi.org/10.1016/j.ijpharm.2020.119686.

[45] A.A. Abd-Elrahman, M.A.E. Nabarawi, D.H. Hassan, A.A. Taha, Ketoprofen mesoporous silica nanoparticles SBA-15 hard gelatin capsules: preparation and in vitro/in vivo characterization, Drug Delivery. 23 (2016) 3387–3398. https://doi.org/10.1080/10717544.2016.1186251.

[46] S. Hendessi, E.B. Sevinis, S. Unal, F.C. Cebeci, Y.Z. Menceloglu, H. Unal, Antibacterial sustained-release coatings from halloysite nanotubes/water borne polyurethanes, Progress in Organic Coatings. 101 (2016) 253–261. https://doi.org/10.1016/j.porgcoat.2016.09.005.

[47] P. Yuan, D. Tan, F. Annabi-Bergaya, W. Yan, M. Fan, D. Liu, H. He, Changes in Structure, Morphology, Porosity, and Surface Activity Of Mesoporous Halloysite Nanotubes Under Heating, Clays and Clay Minerals. 60 (2012) 561–573. https://doi.org/10.1346/CCMN.2012.0600602.

[48] L. Lisuzzo, G. Cavallaro, P. Pasbakhsh, S. Milioto, G. Lazzara, Why does vacuum drive to the loading of halloysite nanotubes? The key role of water confinement, Journal of Colloid and Interface Science 547 (2019) 361–369, https://doi.org/10.1016/j.jcis.2019.04.012

[49] Adi I. Arida, Moawia M. Al-Tabakha, Encapsulation of ketoprofen for controlled drug release, European Journal of Pharmaceutics and Biopharmaceutics 66 (2007) 48-54. https://doi.org/10.1016/j.ejpb.2006.09.010

[50] N. G. Veerabadran, R. R. Price, Y. M. Lvov, Clay nanotubes for encapsulation and sustained release of drugs. Nano 2(2) 115-120 (2007). https://doi.org/10.1142/S1793292007000441

Declaration of interests

☒ The authors declare that they have no known competing financial interests or personal relationships that could have appeared to influence the work reported in this paper.

☐The authors declare the following financial interests/personal relationships which may be considered as potential competing interests:

Credit Author Statement

Dounia Sid: Methodology, Formulations, Writing.

Milad Baitiche: Conceptualization, Review, Supervision.

Ferhat Djerboua: Formulation experiments, Review.

Riadh Bourzami: DRX and TEM characterization.

Mokhtar Boutahala: Conceptualization, Writing, Review, Supervision.

Merir Roufeida: XRF, Zeta potential

A.Gil, Supervision, Review

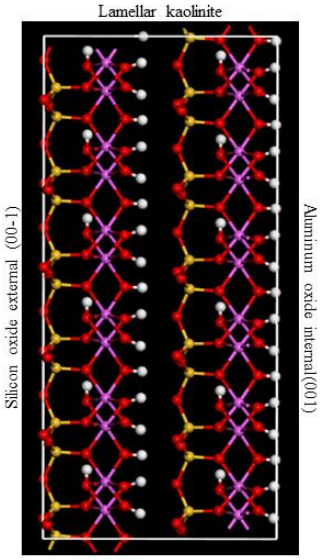

Figure 1: Supercell of kaolinite structure in the direction (001) (3 x 3 x 2).

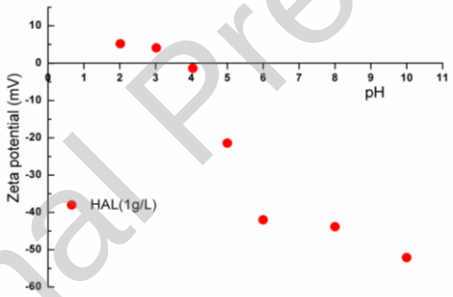

Figure 2: Zeta potential of HAL versus pH

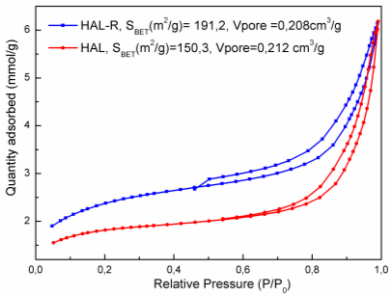

Figure 3: N_2 adsorption/desorption isotherms of HAL-R and HAL

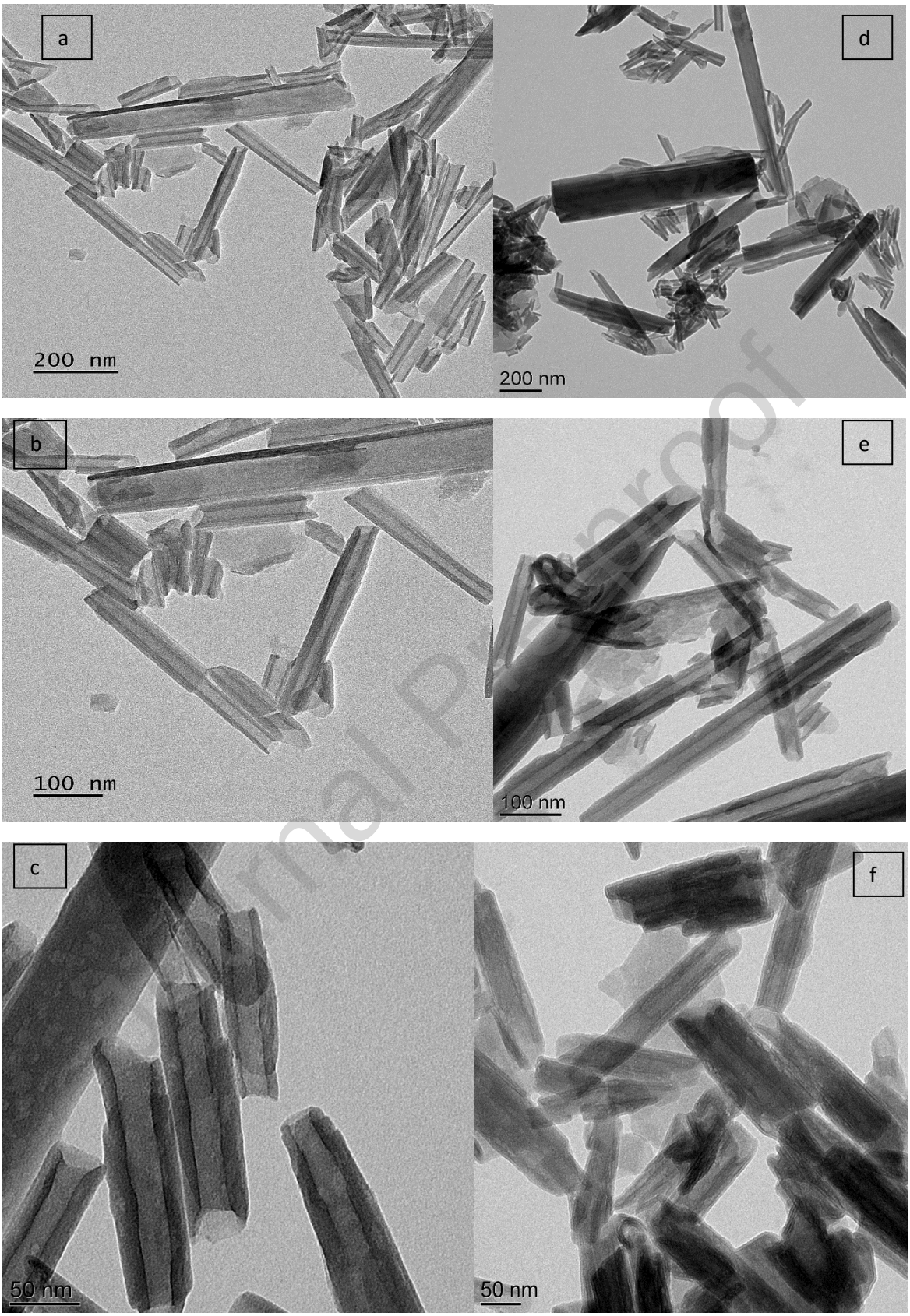

Figure 4: TEM images of (a, b, c) HAL and (d, e, f) HAL-KET

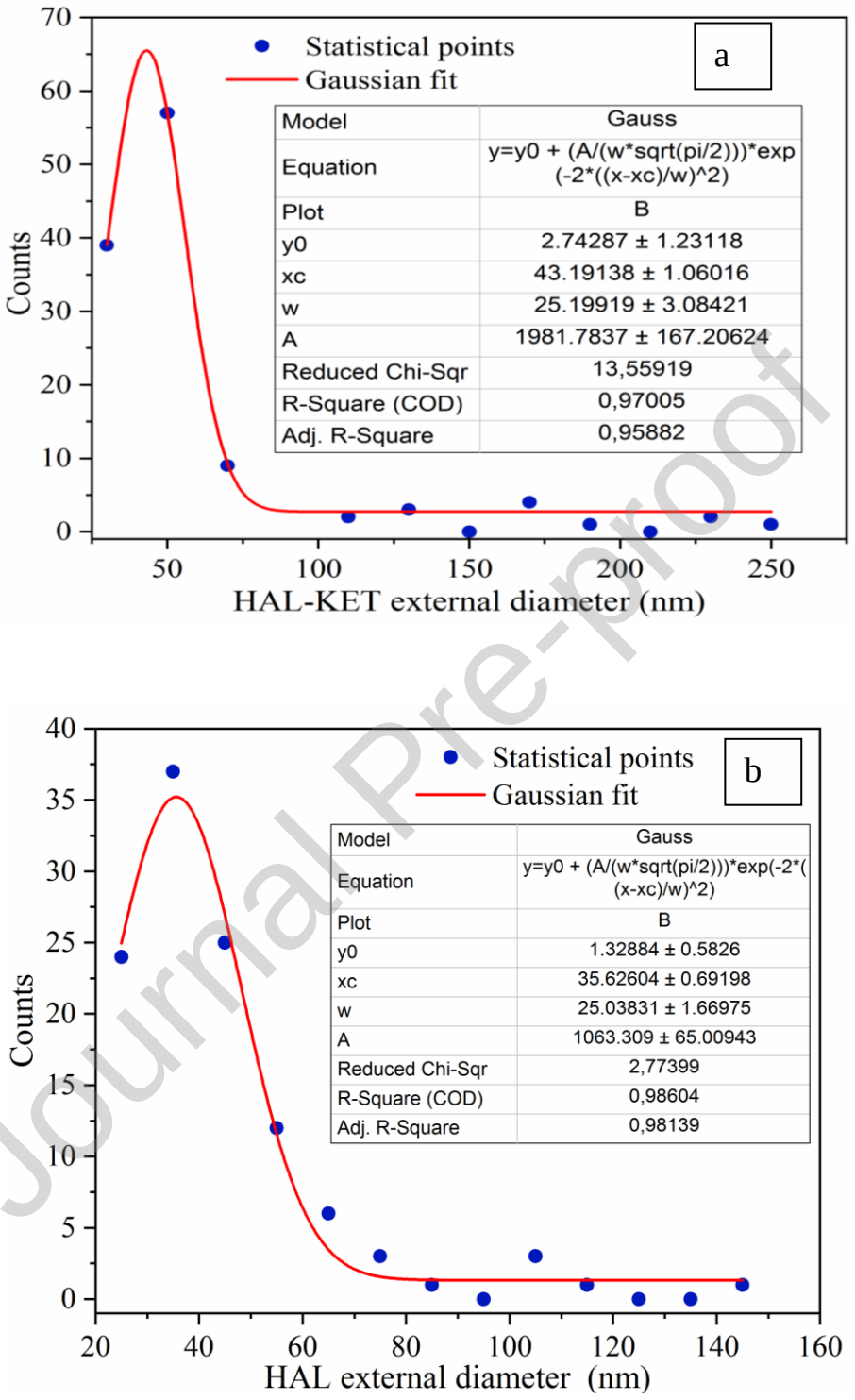

Figure 5: Distribution of the external diameters of (a) HAL-KET and (b) HAL

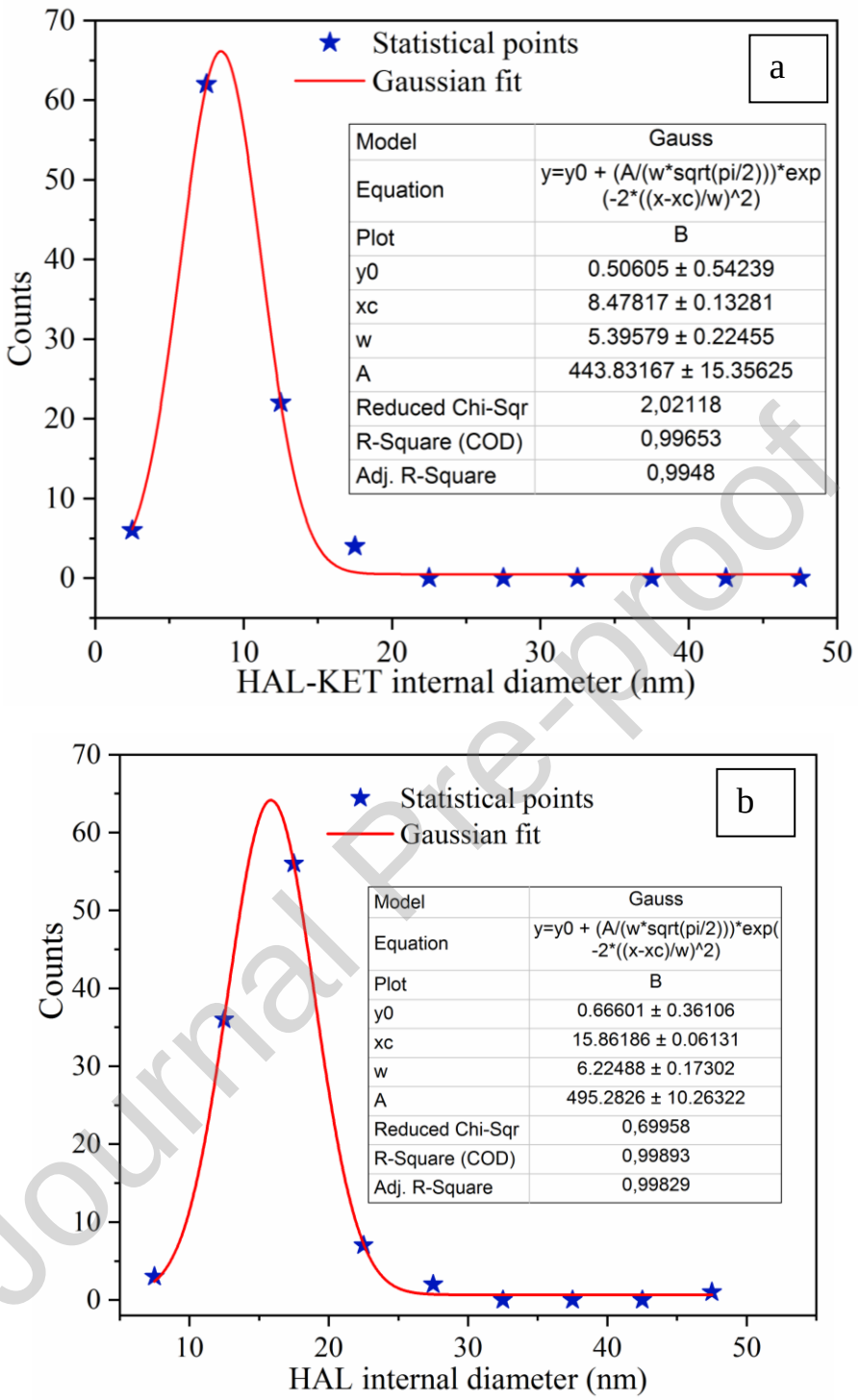

Figure 6: Distribution of the internal diameters of (a) HAL-KET and (b) HAL

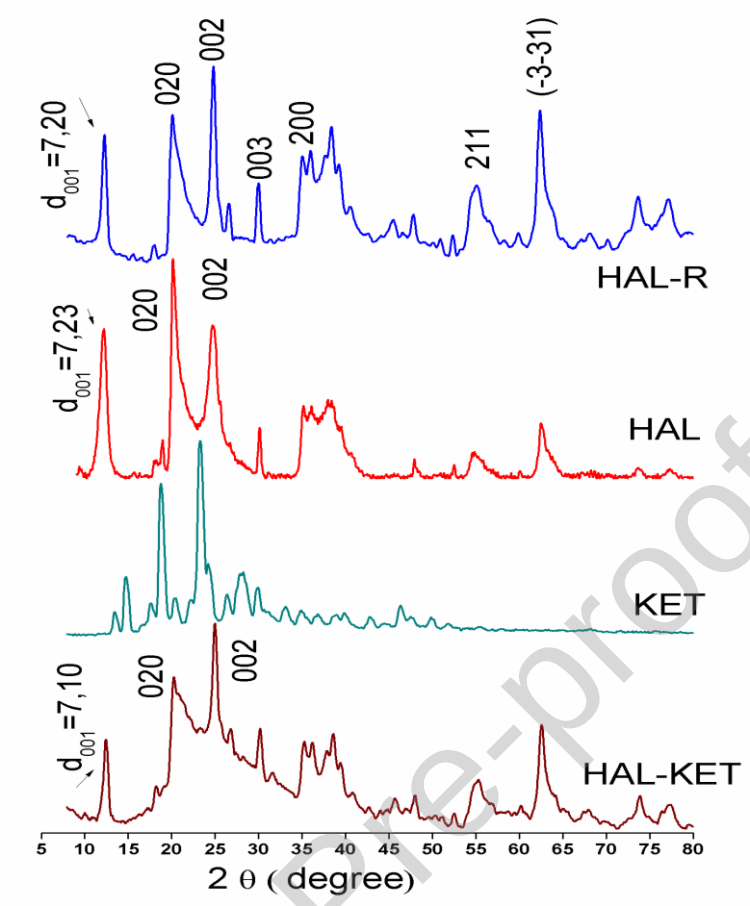

Figure 7: XRD patterns of HAL-R, HAL, KET and HAL-KET provided by the main characteristic plane Miller indices

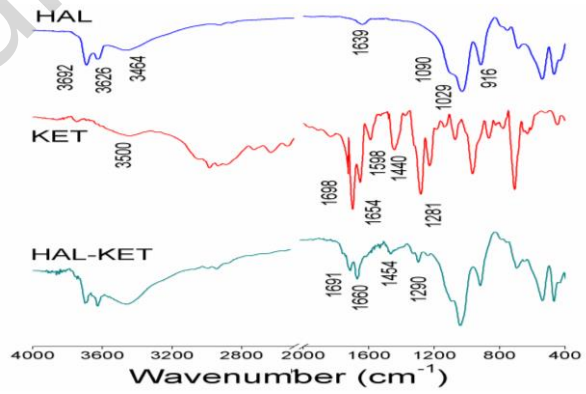

Figure 8: FTIR spectra of HAL, KET and HALKET samples

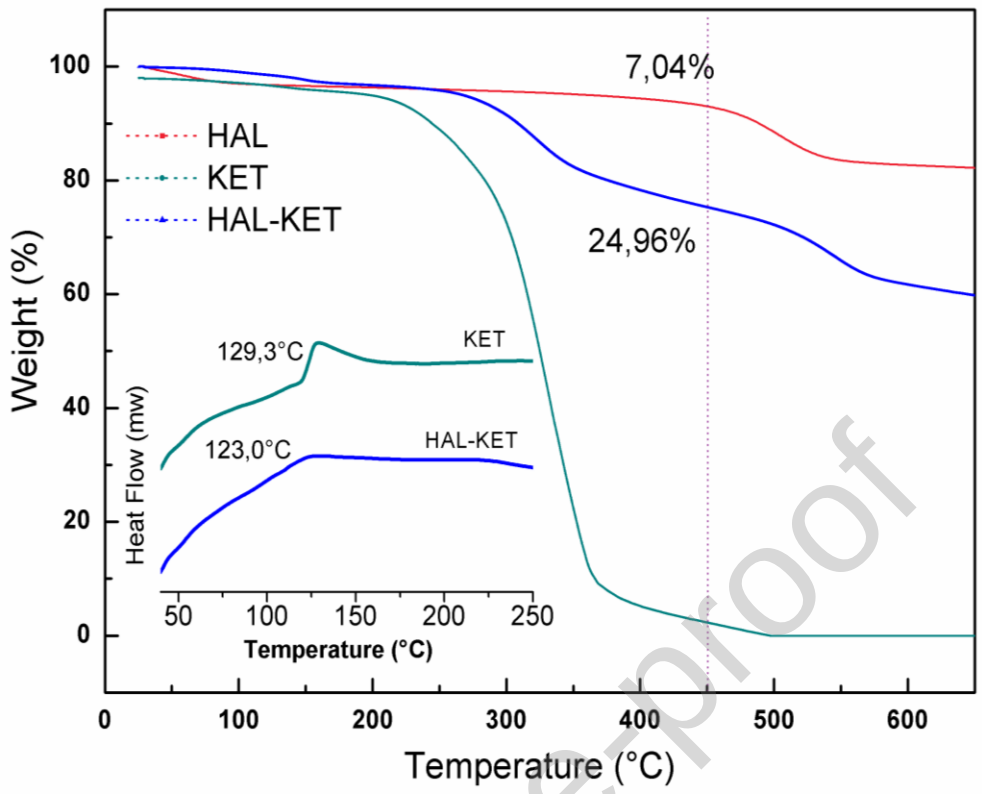

Figure 9: TG analysis of HAL, KET, and HAL-KET and DSC curve (inset)

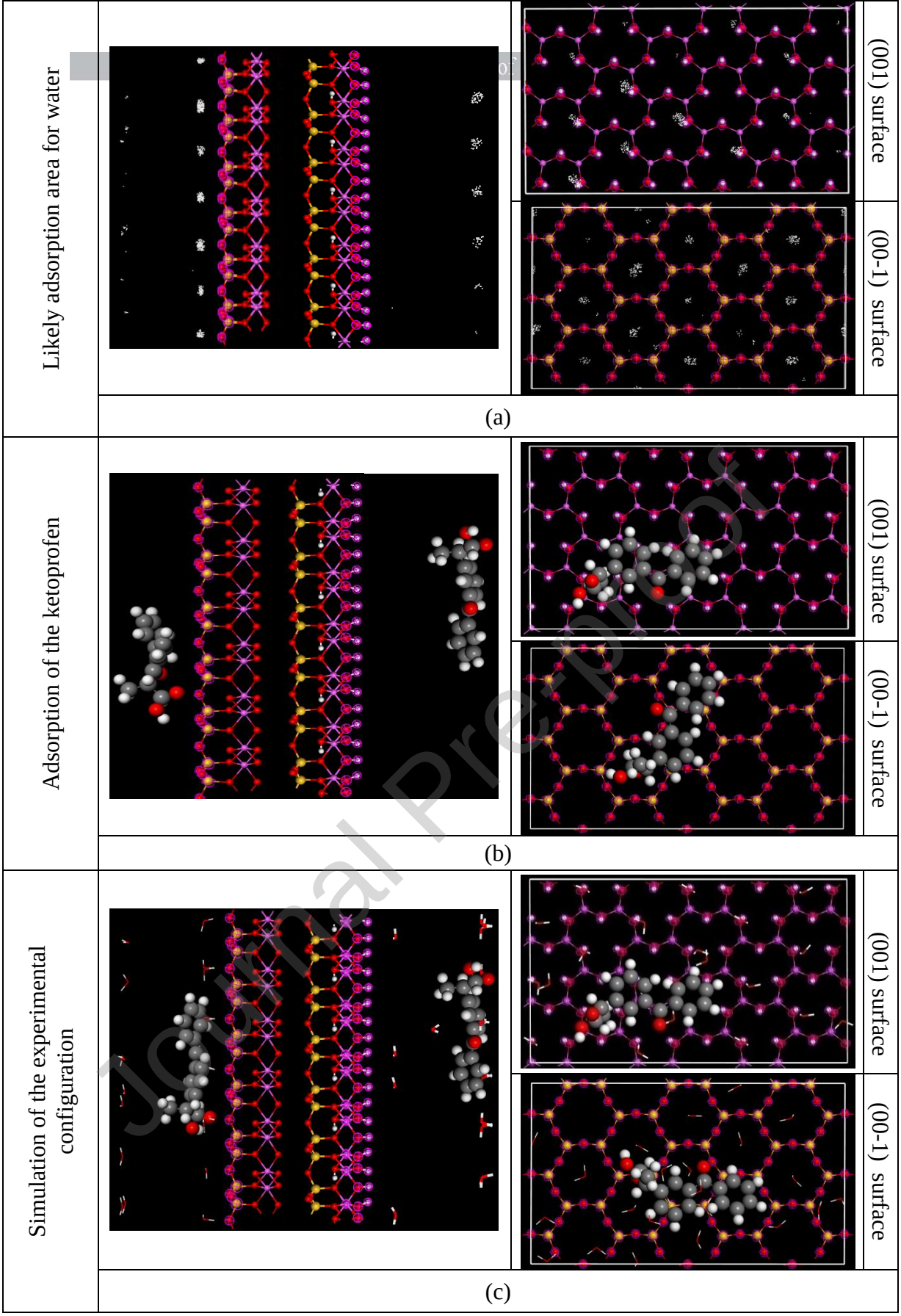

Figure 10: The equilibrium configurations of the KET and water molecules on HAL (100) substrate (a) the most likely adsorption area for the water molecules (b) KET (c) simulation of the experimental configuration.

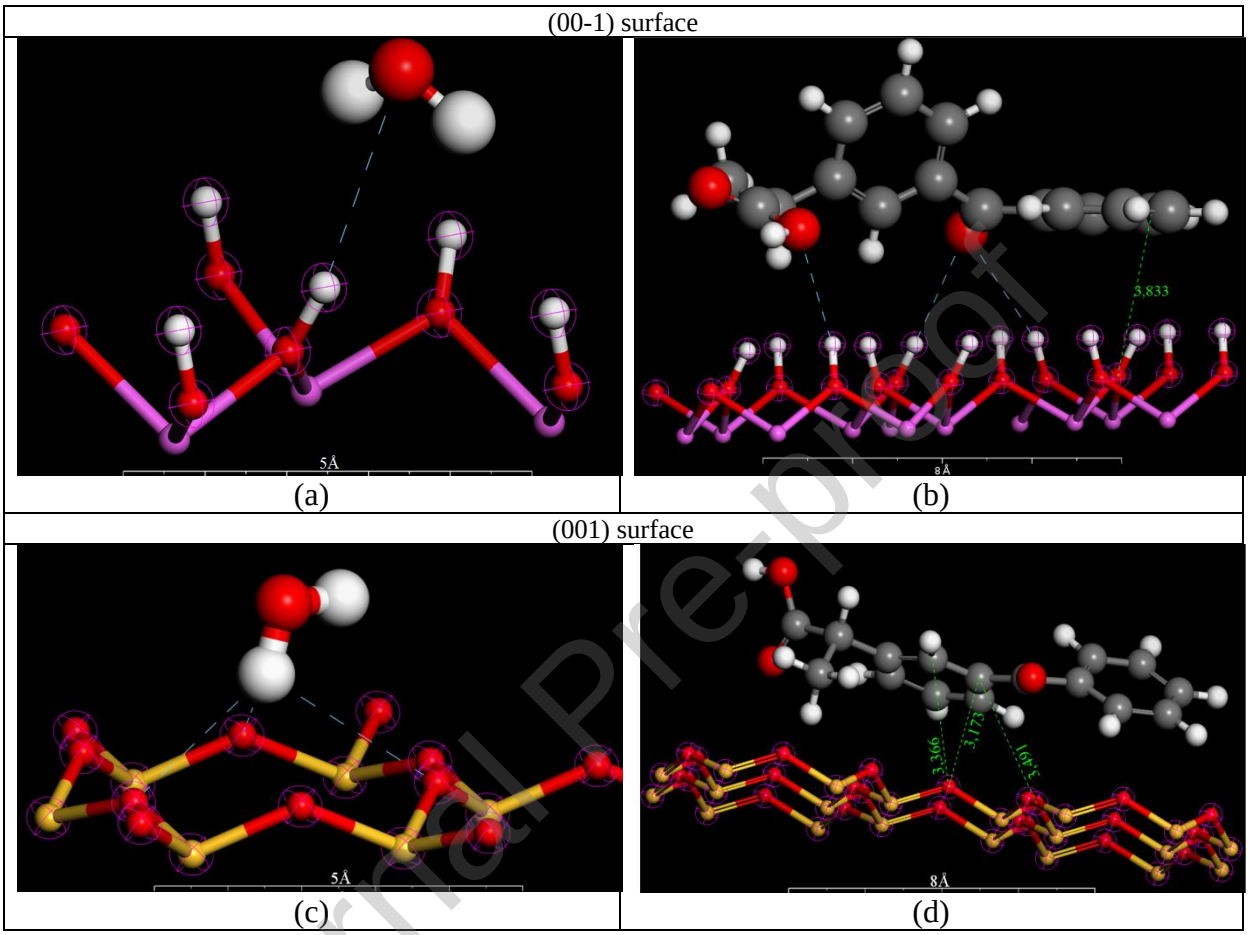

Figure 11: Local magnification of the adsorption configuration, (blue: possible hydrogen bonds, green: distance values).

Graphical abstract

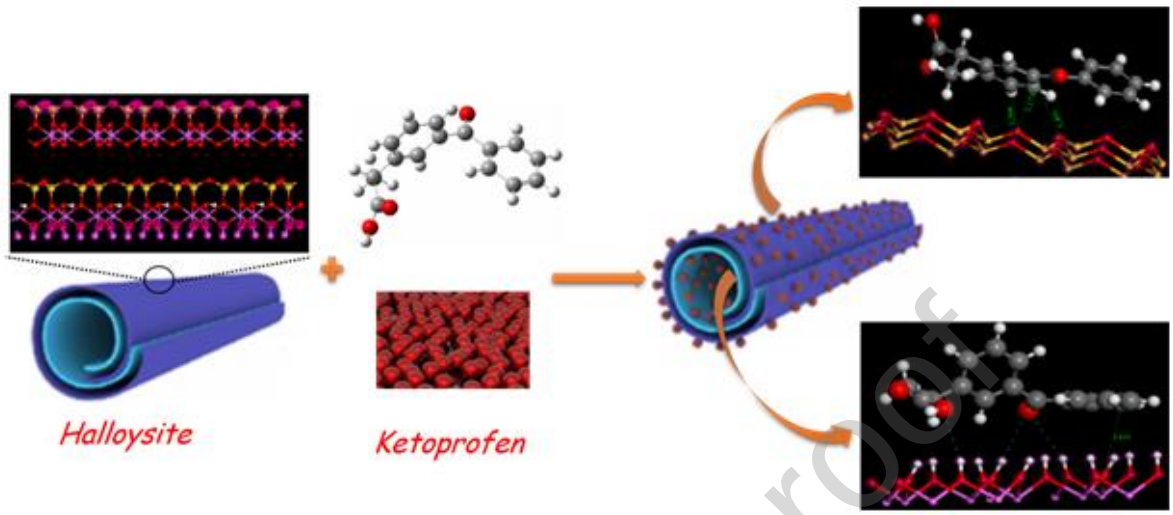

Highlights

- Halloysite was used as a drug carrier for the loading of ketoprofen
- Ketoprofen was successfully loaded to the halloysite with high entrapment efficiency
- The resulting materials were characterized by Zeta potential, N_2 adsorption, XRD, TEM, FTIR, TGA/DSC.
- The classical atomistic molecular simulation method was used for investigated the interaction mechanism between ketoprofen and the halloysite nanotubes.

Table 1: Chemical composition of HAL-R and HAL

	SiO2	Al_2O_3	CaO	Fe_2O_3	K_2O	MgO	MnO	Na_2O	SiO_2/Al_2O_3	Others
HAL-R	49.8	41.4	0.713	0.593	0.586	0.0995	2.35	0.21	1.20	traces
HAL	52.4	40.7	0.174	0.521	0.482	0.105	2.09	0.27	1.29	traces

Table 2: Adsorption energies (kJ/mol) of the ketoprofen and the water molecules

		Total energy	Adsorption energy	Rigid adsorption energy	Deformation energy	Ketoprofen optimization mol : dEad/dNi	Water mol : dEad/dNi
(00-1) surface	Ketoprofen	3.741	-52.686	-35.423	-17.262	-52.686	/
	Water	-3.976	-4.935	-3.976	-0.959	/	-4.935
	Ketoprofen 30 water	-75.77	-151.386	-114.943	-36.442	-58.282	-4.409
(001) surface	Ketoprofen	3.286	-53.141	-36.297	-16.843	-53.141	/
	Water	-4.042	-5.510	-4.042	-1.468	/	-5.510
	Ketoprofen 30 water	-76.375	-162.169	-115.801	-46.368	-60.306	-4.110

Table 3: Geometric parameters of the predicted hydrogen bonds (Angle (°), Bond length (Å))

KET: Ketoprofen. W.: water

		Angle (°)	Bond length (Å)		
		O-H···H	O-H	H···H	D···A
(001)	Ket.	155.959	0.979	2.861	3.776
		166.749	0.983	2.768	3.732
		160.428	0.976	2.820	3.754
	W	147.393	0.979	2.845	3.707
(00-1)	W	140.265	0.989	2.730	3.548
		108.281	0.989	2.789	3.239
		109.070	0.989	2.782	3.243